Ductility of Concrete Beams Reinforced with Both Fiber-Reinforced Polymer and Steel Tension Bars

Linh Van Hong Bui, Boonchai Stitmannaithum, Tamon Ueda

Journal of Advanced Concrete Technology, volume 16 (2018), pp.531-548

Scientific paper

Ductility of Concrete Beams Reinforced with Both Fiber-Reinforced Polymer and Steel Tension Bars

Linh Van Hong Bui[1*], Boonchai Stitmannaithum[2] and Tamon Ueda[3]

Received 21 June 2018, accepted 24 October 2018 doi:10.3151/jact.16.531

Abstract

This paper presents a numerical investigation of the mechanical performance and ductility of concrete beams reinforced by both fiber-reinforced polymer (FRP) and steel tension reinforcement. Three-dimensional (3D) finite element (FE) analysis of beams with both FRP and steel reinforcement was conducted by first using ANSYS to verify the reliability of the FE analysis. The FE analysis can predict the mechanical behavior of the tested beams. To evaluate the ductility of the FRP-steel reinforced concrete (RC) beams considering various factors, such as the effects of the FRP on the steel reinforcement ratio, the location of the FRP reinforcement, the FRP type and the concrete compressive strength, on the mechanical performance of the beams, a parametric study was used to complement the FE analysis. Based on the parametric study, the conditions of the ratio of FRP to steel reinforcement, the location of the FRP reinforcement and the type of FRP reinforcement required to obtain reasonable ductility in practical use were presented.

1. Introduction

Since fiber-reinforced polymer (FRP) reinforcement requires an expensive material, the partial replacement of steel reinforcement by FRP reinforcement is economically feasible. To prevent the corrosion of steel reinforcement in the reinforced concrete (RC) beams in aggressive environments, the most external reinforcement (closest to the concrete surface) could be replaced by FRP reinforcement. In addition, the lack of ductility of FRP composites is a crucial issue affecting the performances of the members reinforced with FRP tension bars. Therefore, concrete beams reinforced by both steel and FRP reinforcements have been considered an interesting topic for experimental and numerical research.

The experimental studies of Aiello and Ombres (2002), Qu *et al.* (2009), Lau and Pam (2010), Ge *et al.* (2015) and Yoo *et al.* (2016) were conducted to investigate deflection, curvature, ductility, crack width of concrete beams with hybrid usage of FRP and steel tension reinforcement. Their studies indicated that the hybrid usage of steel and FRP reinforcement was more advantageous in the consideration of deformability than the use of steel reinforcement. Generally, adding conventional steel bars could improve the flexural ductility of hybrid FRP-steel RC members. In another aspect, the crack width and spacing values were decreased with the presence of steel reinforcement in comparison with the crack width and spacing attained by beams reinforced with only FRP bars. The average crack spacing of the hybrid FRP-steel RC beams was in the middle of the average crack spacing of the steel RC beams and FRP RC beams.

Aiello and Ombres (2002) showed that using the moment-curvature law could accurately predict the behavior of concrete beams reinforced by steel and FRP bars, and the American Concrete Institute (ACI) code (ACI 440.1R-06, 2006) furnished a good prediction of the deflections and crack width in the serviceability phase. Aiello and Ombres (2002) also offered a design model to determine the effective moment of inertia for steel RC beams and FRP RC beams based on the calibration of the experimental results. However, Qu *et al.* (2009) adopted the model of Bischoff (2007), which was initially studied by Branson (1977), to calculate the deflection of concrete beams reinforced with glass fiber-reinforced polymer (GFRP) and steel bars at the service load level.

By conducting an experimental and theoretical program, Qu *et al.* (2009) and Lau and Pam (2010) discovered that the use of steel reinforcement in combination with GFRP bars enhanced the flexural performance of GFRP RC beams. The studies by Qu *et al.* (2009) and Ge *et al.* (2015) proposed equations to compute the flexural moment capacity and strength of FRP bars for hybrid FRP-steel RC beams. The axial stiffness ratio between GFRP and steel bars had little influence on flexural capacity, whereas the effective reinforcement ratio was a reasonable parameter for evaluating the ultimate moment of hybrid FRP-steel RC beams. For the failure mode prediction of hybrid FRP-steel RC beams, the balanced effective reinforcement ratio could be em-

[1]Ph.D. Student, Department of Civil Engineering, Chulalongkorn University, 254 Phayathai Road, Pathumwan, Bangkok 10330, Thailand.
*Corresponding author, *E-mail:* bvhlinh@gmail.com
[2]Professor, Department of Civil Engineering, Chulalongkorn University, 254 Phayathai Road, Pathumwan, Bangkok 10330, Thailand.
[3]Professor, Laboratory of Engineering for Maintenance System, Hokkaido University, Sapporo, Hokkaido Prefecture 060-0808, Japan.

Table 1 Properties of the tested beams.

Study	Beam ID	A_s (mm^2)*	A_f (mm^2)*	$\rho_r = A_f/A_s$
Aiello and Ombres (2002)	A1	100.48 (2d8)	88.36 (2d7.5)	0.8789
	A2	100.48 (2d8)	157.08 (2d10)	1.5625
	A3	226.19 (2d12)	235.62 (3d10)	1.0417
Qu *et al.* (2009)	B1	452.16 (4d12)	-	-
	B2	-	506.45 (4d12.7)	-
	B3	226.08 (2d12)	253.23 (2d12.7)	1.1201
	B4	200.96 (1d16)	396.91 (2d15.9)	1.9751
	B5	401.92 (2d16)	141.69 (2d9.5)	0.3525
	B6	401.92 (2d16)	253.23 (2d12.7)	0.6301
	B7	113.04 (1d12)	141.69 (2d9.5)	1.2535
	B8	1205.76 (6d16)	396.91 (2d15.9)	0.3292
Lau and Pam (2010)	G0.6-T1.0-A90**	981.75 (2T25)	567.06 (2G19)	0.5776
	G1.0-T0.7-A90**	628.32 (2T20)	981.75 (2G25)	1.5625
	G0.3-MD1.0-A90**	981.75 (2MD25)	283.53 (1G19)	0.2888

*A_s and A_f: The area of the steel and AFRP tension reinforcement, respectively
**MD, T, G, and A90: The mild steel, high yield steel, GFRP reinforcement, and 90^o hook angle in stirrups respectively

ployed. Based on the results of Lau and Pam (2010), the requirements for the minimum GFRP flexural reinforcement given by the ACI code could be reduced by approximately 25%.

Together with the experimental program, the numerical and analytical investigations such as Faza and GangaRao (1993), Tan (1997), Zhang *et al.* (2012), Kara *et al.* (2015, 2016), Hawileh (2015), Oller *et al.* (2015), Yoo and Banthia (2015), Bencardino *et al.* (2016), Zhang *et al.* (2016) and Qin *et al.* (2017) were conducted to propose the design method for concrete beams reinforced/strengthened by both FRP and steel tension reinforcement, and determining the curvature, deflection, ductility and moment capacity of hybrid FRP-steel RC beams. Most of those studies showed good agreement of the numerical and analytical results in the comparison with the experimental results. However, several important parameters were not studied in the past experiments and the previous FE simulations. The ductility evaluation of the hybrid FRP-steel RC beams is limited because of the lack of the research data and has not achieved the high reliability. This study, therefore, presents a numerical investigation on the structural behavior of concrete beams reinforced with FRP-steel bars under various conditions. The main contents of this study are as follows: (1) FE simulation of beams with hybrid usage of FRP and steel reinforcement, with experimental data available to show the reliability of FE simulation results, (2) the parametric study by the FE simulation on ductility of beams reinforced with both FRP and steel tension reinforcement, and (3) the ductility analysis with ductility index to show feasible hybrid use of FRP-steel tension reinforcement.

2. Experimental data to validate the finite element (FE) models

The data in the experimental program of Aiello and Ombres (2002), Qu *et al.* (2009), Lau and Pam (2010) were adopted to verify the FE models. Aiello and Ombres (2002) presented an experimental investigation of five concrete beams (150 x 200 x 3000 mm^3) reinforced by both aramid fiber-reinforced polymer (AFRP) and steel reinforcement. One beam was reinforced by only AFRP bars, another one was reinforced with only steel reinforcement, and three others were reinforced with a hybrid AFRP-steel reinforcement. Four-point flexural loading tests were conducted on the beams. All the beams used the two steel bars of 8 mm diameter as the compression reinforcement, and transverse reinforcement with 8 mm diameter and 100 mm spacing were employed as shear reinforcement. More details of the beams in the work by Aiello and Ombres (2002), which are investigated in the present study, are shown in **Fig. 1** and **Table 1**.

Qu *et al.* (2009) studied the flexural behavior of concrete beams reinforced with both GFRP and steel bars. This research employed eight concrete beams (180 x

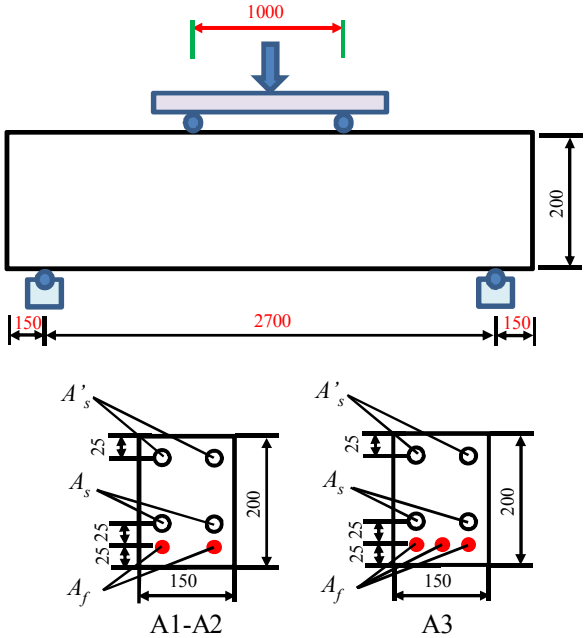

Fig. 1 Geometrical dimension of the tested beams. (Aiello and Ombres 2002)

250 x 1800 mm^3), including two control beams reinforced with only steel or only GFRP bars, and six hybrid FRP-steel RC beams. All beams used two steel bars of 10 mm diameter as the compression reinforcement as well as steel stirrups with 10 mm diameter and 100 mm spacing. A four-point flexural loading test was conducted. In the following year, Lau and Pam (2010) studied the twelve specimens, simply supported and subjected to a point load at midspan, including plain concrete beams, steel-reinforced concrete beams, pure GFRP RC beams, and hybrid GFRP-steel RC beams. The two steel bars of 6 mm diameter were employed as the compression reinforcement, steel stirrups with 8 mm diameter and 50 mm spacing at the two ends of beams and 100 mm spacing at the rest of beams were applied as shear reinforcement. **Figures 2** and **3** and **Table 1** show the more details of the beam specimens tested by Qu *et al.* (2009) and Lau and Pam (2010), which are numerically investigated in the present study.

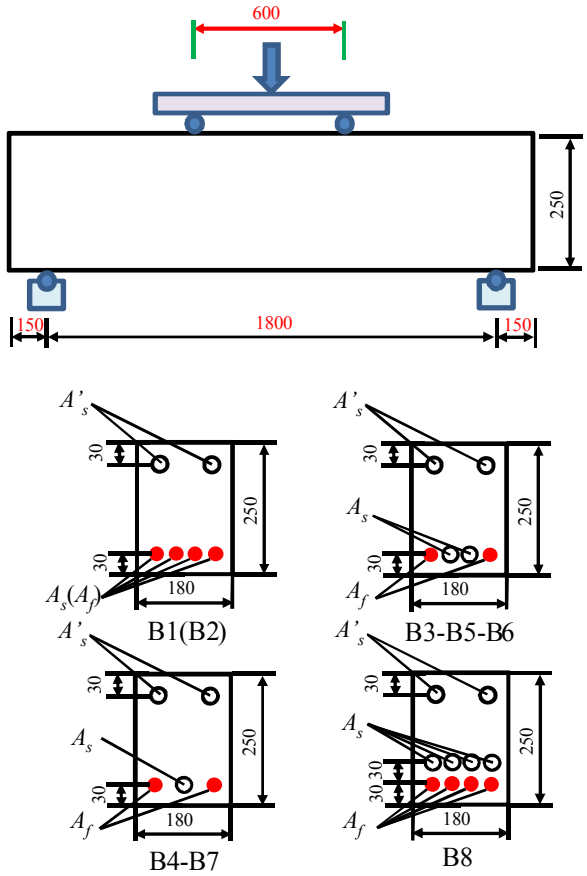

Fig. 2 Geometrical dimension of the tested beams. (Qu *et al.* 2009)

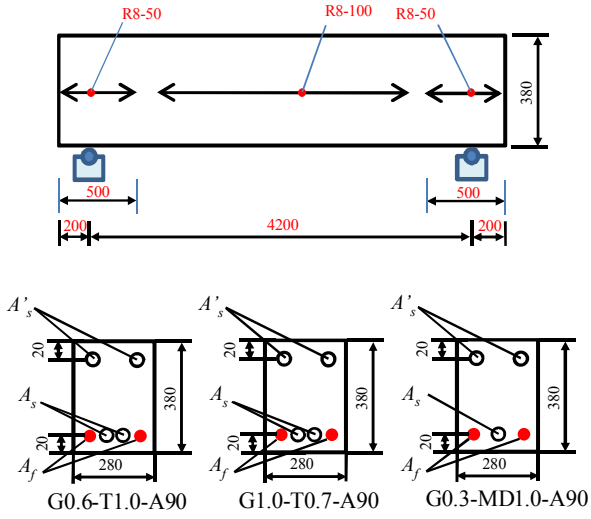

Fig. 3 Geometrical dimension of the group tested beams. (Lau and Pam 2010)

3. Validation of three-dimensional (3D) finite element (FE) models

3.1 Finite element program

In this study, numerical analyses were conducted by a commercially available software, ANSYS 15.0. A quarter FE model was applied to investigate the performance of the tested beams based on the symmetrical condition as shown in **Fig. 4**. For this investigation, the mesh discretization is 10 x 10 mm^2. In addition, the descriptions of the element types and material models for the FE program follow from the previous work (Linh *et al.* 2017) of the authors of the present study.

(1) Element types

SOLID65, LINK180 and SOLID45 are used as the ANSYS 15.0 elements for nonlinear 3D modeling of concrete materials, reinforcement and elastic steel support, respectively. The SOLID65 element is capable of modeling of concrete cracking in tension and crushing in compression. The SOLID65 element is also defined by eight nodes, and each node has three degrees of freedom that are the translations in the nodal x, y, and z directions (Linh *et al.* 2017). However, LINK180 is a uniaxial tension-compression element with three degrees of freedom at each node that are the translations in the nodal x, y, and z directions (Linh *et al.* 2017). In addition to SOLID45, which is applied to model the supporting and loading plates, the software that is used for the three-dimensional modeling of solid structures and the definition of the SOLID45 element is similar to that of the SOLID65 element except for the capability of cracking in tension and crushing in compression (Hawileh 2015; Linh *et al.* 2017). The perfect bond behavior between reinforcement and concrete is assumed in the FE models.

(2) Material models

Various constitutive models have been employed in FE simulations of hybrid FRP-steel RC beams to describe the behavior of concrete under a wide range of complex stress and strain histories. These models included nonlinear elastic models and plasticity-based models whether perfect plasticity models or elastic–plastic models (Godat *et al.* 2012). In this study, the model of

Hognestad *et al.* (1955) is adopted to simulate the nonlinear response of concrete in compression. Equation (1) and **Fig. 5(a)** show more details of the Hognestad *et al.* (1955) parabola.

$$f_c = f_c'\left[2\left(\frac{\varepsilon}{\varepsilon_0}\right)-\left(\frac{\varepsilon}{\varepsilon_0}\right)^2\right] \quad (1)$$

where

f_c is the compressive stress of the concrete (MPa) corresponding to the specified strain, ε,

f_c' is the concrete compressive strength (MPa),

$\varepsilon_0 = \frac{2f_c'}{E_c}$, and E_c is the elastic modulus of the concrete (MPa).

Linh *et al.* (2017) showed the concrete behavior in tension according to the model of William and Warnke, which was recommended by the ANSYS software. **Figure 5(b)** shows the stress-strain relationship of concrete under tension. At first, the linear elasticity to the concrete tensile strength is used for concrete behavior in tension. Then, a steep drop in the concrete tensile stress by 40% is the stress relaxation in tension. The rest of model is represented as the curve that descends linearly to zero tensile stress at a strain value six times larger than strain value at the concrete tensile strength (Hawileh 2015). On the other hand, the steel reinforcement is described as the elastic fully plastic model based on the von Mises yield criterion, while the FRP bars are simulated as elastic-brittle materials until rupture. **Figure 6** shows the stress-strain relationships of steel and FRP reinforcement that are applied in the FE simulations. Moreover, the mechanical properties of concrete, steel, and FRP reinforcement of all the investigated beams taken from the above three past studies shown in **Table 2**.

3.2 Results and discussion

To verify the reliability of the FE method, the concrete beams reinforced by steel, FRP, and steel-FRP tension reinforcements in Chapter 2 were simulated, and the simulation results are investigated. The failure definition

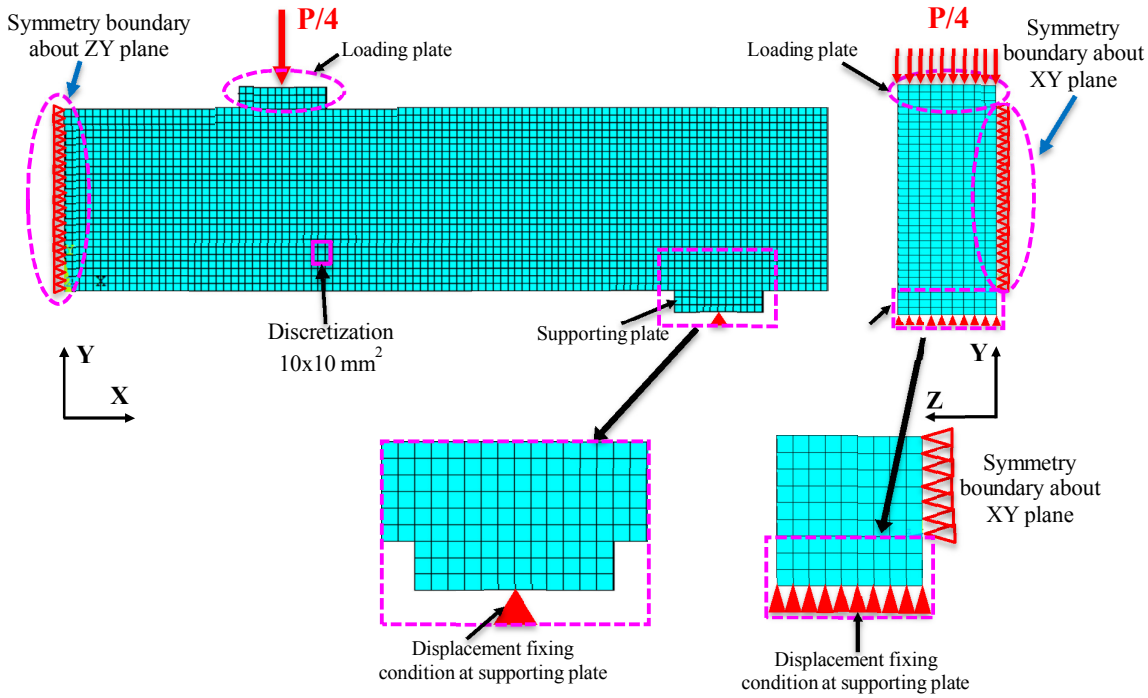

Fig. 4 A quarter typical FE model for numerical program by using ANSYS 15.0.

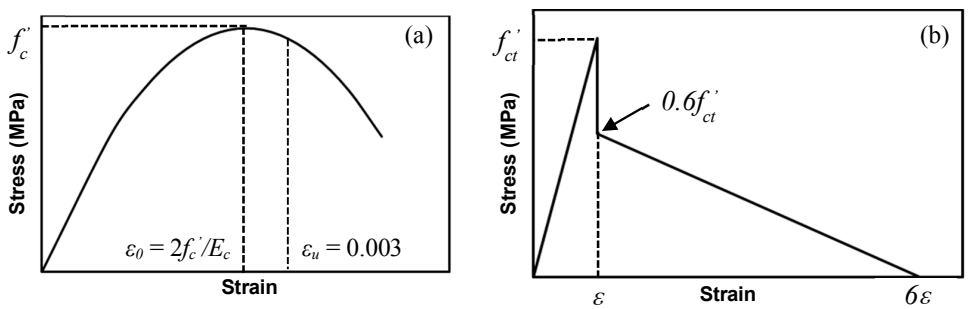

Fig. 5 Models of concrete in (a) compression and (b) tension.

Table 2 Mechanical properties of materials.

Study	Beam ID	f_c' (MPa)	E_c (GPa)	f_y (MPa)	f_{fu} (MPa)	E_f (MPa)	ρ_s (%)	ρ_f (%)
Aiello and Ombres (2002)	A1	45.7	34.7	558	1674	49000	0.335	0.294
	A2	45.7	34.7	558	1366	50100	0.335	0.523
	A3	45.7	34.7	558	1366	50100	0.754	0.785
Qu *et al.* (2009)	B1	30.95	30.9	363	NA	NA	1.142	NA
	B2			NA	782	45000	NA	1.280
	B3	33.10	31.5	363	782	45000	0.571	0.640
	B4			336	755	41000	0.508	1.003
	B5	34.40	31.9	336	778	37700	1.015	0.358
	B6			336	782	45000	1.015	0.640
	B7	40.65	33.5	363	778	37700	0.286	0.358
	B8			336	755	41000	3.269	1.076
Lau and Pam (2010)	G0.6-T1.0-A90	44.6	34.5	550	588	39500	0.923	0.533
	G1.0-T0.7-A90	39.8	33.3	597	582	38000	0.591	0.923
	G0.3-MD1.0-A90	41.3	33.7	336	588	39500	0.923	0.266

Each study is indicated: beam ID, concrete compressive strength (f_c'), elastic modulus of concrete (E_c), steel yielding strength (f_y), ultimate strength and elastic modulus of FRP reinforcement (f_{fu}, E_f), reinforcement content of steel and FRP bars are ρ_s and ρ_f, respectively.

Table 3 Experimental and numerical results on load carrying capacity, absorption energy and failure mode.

Authors	Beam ID	$P_{exp.}$ (kN) (Absorption energy (kNmm))	$P_{num.}$ (kN) (Absorption energy (kNmm))	Difference in load (%)	$\rho_r = A_f/A_s$	Failure mode	
						Experiment	Simulation
Aiello and Ombres (2002)	A1	58 (3516.0)	59 (3658.6)	1.72	0.8789	SY-CC*	SY-CC
Qu *et al.* (2009)	B1	108 (1816.9)	112 (2076.6)	3.70	-	SY-CC	SY-CC
	B2	145 (2520.9)	132 (2449.1)	8.97	-	CC	CC
	B3	127 (2669.4)	128 (2937.3)	0.79	1.1201	SY-CC	SY-CC
	B4	129 (2330.8)	126 (2602.0)	2.33	1.9751	SY-CC	SY-CC
	B5	125 (2864.8)	120 (2888.4)	4.00	0.3525	SY-CC	SY-CC
	B6	140 (2512.3)	127 (2366.3)	9.29	0.6301	SY-CC	SY-CC
	B7	78 (1892.4)	85 (1777.5)	8.97	1.2535	SY-CC	SY-CC
Lau and Pam (2010)	G0.6-T1.0-A90	220 (13920.6)	204 (13576.4)	7.27	0.5776	SY-CC	SY-CC
	G0.3-MD1.0-A90	141 (6506.0)	154 (7608.9)	9.22	0.2888	SY-CC	SY-CC

*SY and CC: The steel yielding and concrete crushing, respectively

of beam specimens in the FE analysis is, after steel yielding, either the stress in FRP reinforcement reaching their rupture strength or the concrete compressive strain exceeding 0.003. The structural performances of the hybrid FRP-steel RC beams in terms of load-deflection response and failure modes of the FE models are compared with the results obtained from the corresponding experimental data. In addition, the stress of reinforcement and crack propagation at the load steps of a representative beam B3 are also described.

Figure 7 shows the load-midspan deflection curves of experimental and simulated results for the ten beam specimens with the one steel RC beam, one pure FRP RC beam, and eight hybrid FRP-steel RC beams. It is explicit that the FE results attain the good appraisal in the comparison with the tested data, and a maximum deviation less than 10% not only in the load-carrying capacity but also in the displacement is easily found from **Fig. 7** and **Table 3**. On the other hand, **Figs. 8** and **9** show the stress distribution and cracking pattern in the hybrid FRP-steel RC beam (B3) as an example. In general, the load-displacement curves from the FE analysis

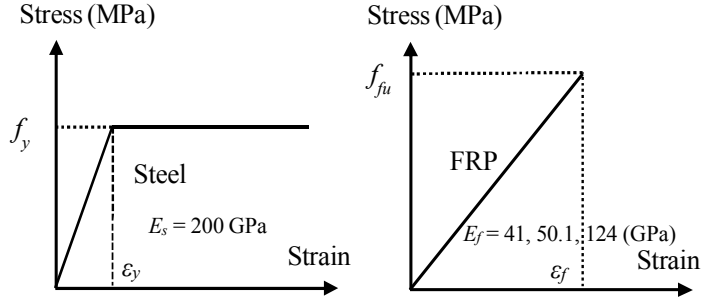

Fig. 6 Stress-strain relationships of steel and FRP reinforcement.

are slightly stiffer than the load-displacement curves from the experimental results. One of the reasons is the perfect bond assumption between reinforcement and concrete in the FE model. The effects of the concrete shrinkage, which may cause cracking, are not considered in the simulation, which is possibly another cause of this overestimated stiffness. Moreover, the fact of not considering shrinkage also results in the higher cracking load in the specimens from the FE analysis compared to the cracking load in the beams from the tests, which might be reduced by the drying shrinkage. On the other hand, by using FRP bars, the load-carrying capacity of the hybrid FRP-steel RC beam increases because the FRP strength is higher than that of steel, and the overall beam behavior changes to be more brittle due to the lack of plasticity of FRP. As shown in **Table 3**, the simulated beams fail in the concrete crushing after steel yielding, and this failure mode is also indicated in the experimental program in the literature. Evidence for this statement is shown in **Fig. 8(a),** in which the stress of the FRP bar in the beam B3 is less than the rupture values. Similarly, at the ultimate load, the steel reinforcement yields (**Fig. 8(b)**) and after the diagonal cracking zone is formed (**Fig. 8(d)**), the concrete is crushed (**Figs. 8(c)**, **8(d)** and **9**). All beams in this investigation are designed to fail upon the concrete crushing; therefore, the strength in the FRP bars is reserved, and plastic deformation of the concrete is allowed. As seen in the experimental and numerical comparison (**Fig. 7**), since the load applied to the beam after steel yielding is all taken up by the FRP reinforcement and the concrete, the slopes of the curves before and after steel yielding of the hybrid FRP-steel RC beams change more gradually.

Furthermore, the crack propagation at the applied load stages and the general response of the concrete beams with the hybrid use of FRP and steel reinforcement are exhibited in **Figs. 9** and **10**, respectively. **Figure 9** shows the zones where specific cracking takes place, which are represented by a circle that appears when a principal tensile stress exceeds the ultimate tensile strength of the concrete. In stage 1, tensile concrete is cracked, and the steel and FRP reinforcement are beginning to activate under the increase in the applied load (as shown in **Fig. 7**). Then, the concrete cracking zone propagates vertically and then horizontally to the two ends of the beams. As demonstrated in **Fig. 10**, until the

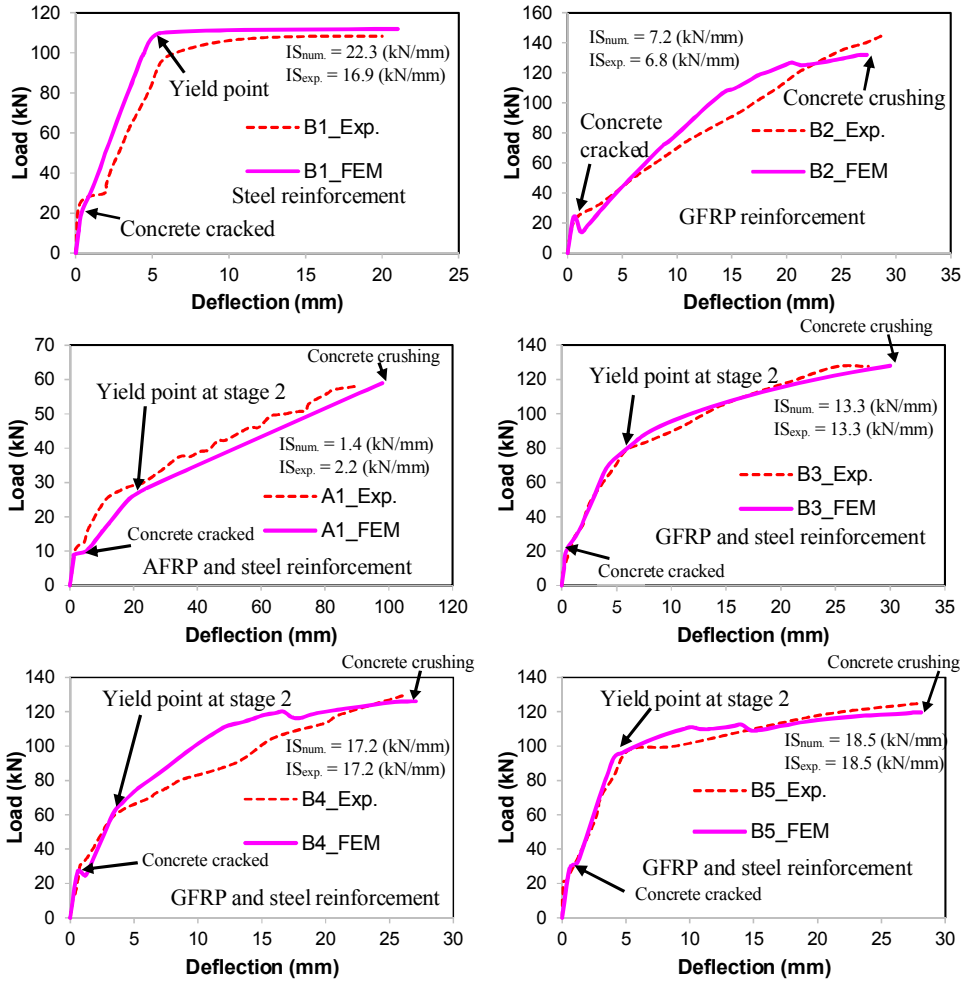

Fig. 7 Comparison of load-midspan deflection relationship between the tested and FE results: the first two specimens are steel and FRP RC beams, respectively, and the remaining specimens are hybrid beams.

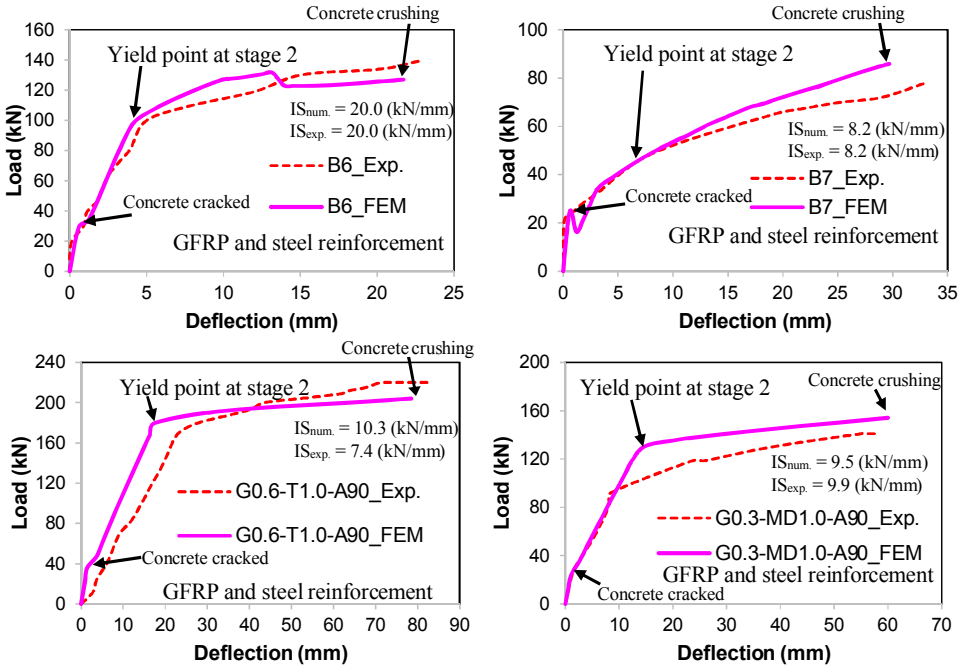

Fig. 7 Comparison of load-midspan deflection relationship between the tested and FE results: the first two specimens are steel and FRP RC beams, respectively, and the remaining specimens are hybrid beams (continued)

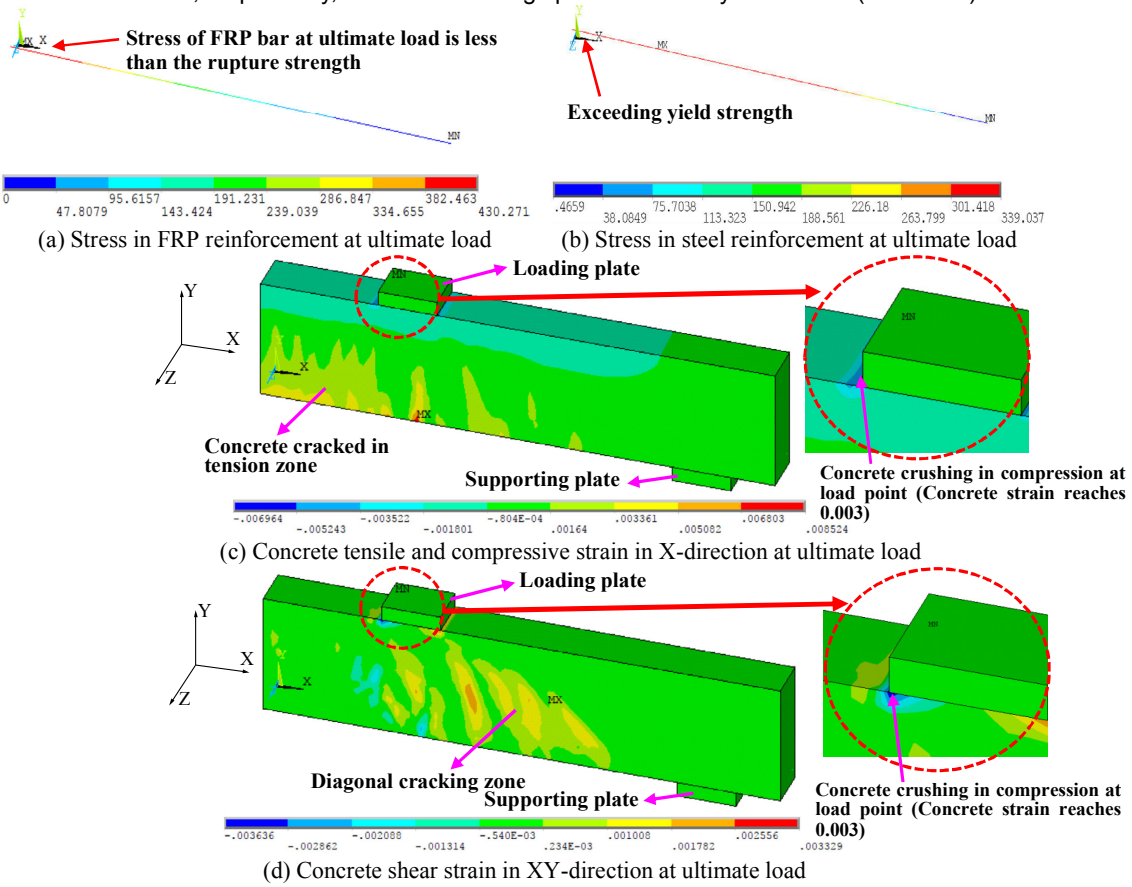

(a) Stress in FRP reinforcement at ultimate load

(b) Stress in steel reinforcement at ultimate load

(c) Concrete tensile and compressive strain in X-direction at ultimate load

(d) Concrete shear strain in XY-direction at ultimate load

Fig. 8 Stress in FRP bar, stress of steel reinforcement, and concrete strain at ultimate load of the representative hybrid beam B3.

steel reinforcement yields, FRP reinforcement works slightly. This is the behavior of hybrid FRP-steel RC beams at the end of stage 2, and the yielding point of each analyzed specimen is also presented in **Fig. 7**. In stage 3, in which the steel reinforcement yields, FRP is significantly activated, and concrete is crushed in the compression zone, resulting in the failure of the hybrid FRP-steel RC beam (as indicated in **Fig. 7**).

It was also observed from the experimental study by Aiello and Ombres (2002), for the hybrid FRP-steel RC beams, the crack spacing and the crack width are lower than those of the beams with single FRP reinforcement. This fact is mainly due to the presence of steel bars in the combined FRP-steel beams which allows the reduction of strain in FRP reinforcement, resulting in the less crack width and spacing. In addition, from **Fig. 11**, the FE investigation of the strain distribution through the height at the midspan section of beams B5, B6 and B7 at the load levels of 80% of ultimate load for B5 and 50% of ultimate load for B6 and B7 demonstrates a good agreement with the strain distribution through the depth at corresponding section of those specimens measured in the experiment. Obtained results from the comparison imply that the assumption of the plane cross section was still effective for concrete beams with hybrid use of steel and FRP tension reinforcement, because the strain distribution in concrete and longitudinal reinforcement were nearly proportional to the distance from the neutral axis.

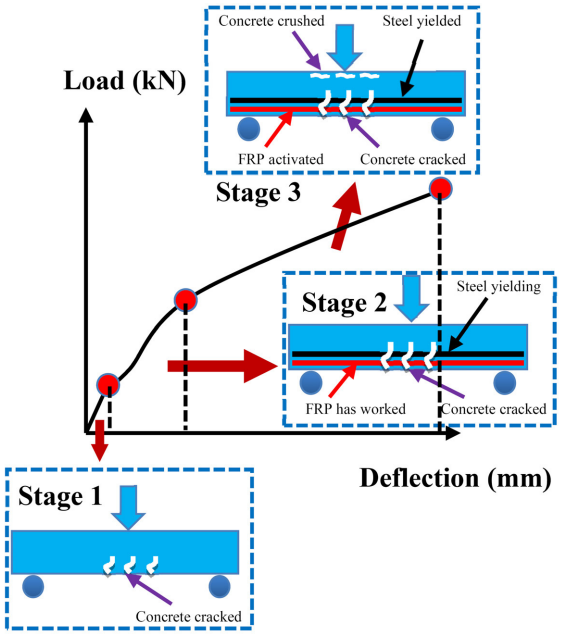

Fig. 10 General behavior of hybrid beams.

To further validate the simulated results with the tested data, consider the analyzed beams in terms of the absorption energy, which is defined as the area under the load-displacement diagrams and is shown in **Table 3**. The energy values computed by the numerical results are close to the absorption energy values calculated from the experimental data. In addition, it is also obvious from **Fig. 7** that the initial stiffness (IS), which is estimated by the ratio of load to deflection at the yield point, of the investigated beams computed from experimental data is close to the values of the initial stiffness calculated from the numerical results. Observing the

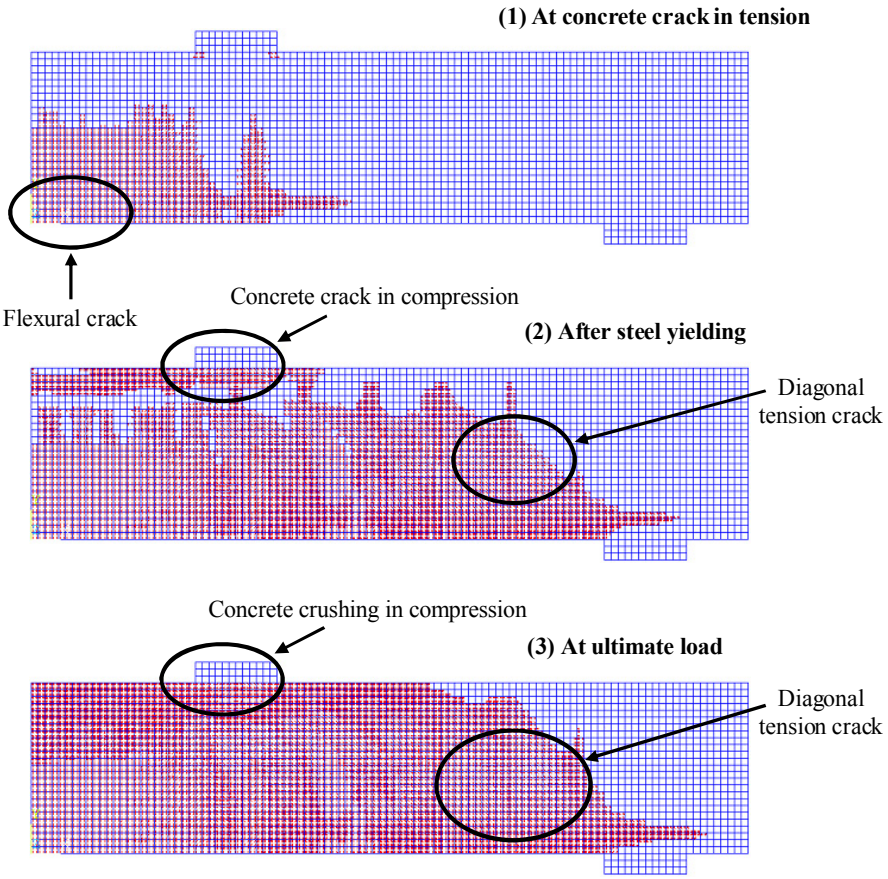

Fig. 9 Crack propagation under the load stages of the representative hybrid FRP-steel RC beam B3.

trend of the values of the initial stiffness in **Fig. 7**, the initial stiffness of the specimens is governed by the reinforcement ratio of A_f/A_s. The lower hybrid reinforcement ratios A_f/A_s result in the higher initial rigidity, and the beam reinforced with single steel tension bars provides the highest stiffness. Moreover, the trend of the absorption energy values presented in **Table 3** implies that the ductility of the beams reinforced by steel and FRP tension bars is also decided by the reinforcement ratio A_f/A_s. The use of the low ratio of FRP to steel ($\rho_r = A_f/A_s$) results in the higher absorption energy, therefore the beams with small hybrid reinforcement ratio offer the enhancement of the ductility and initial rigidity of the hybrid FRP-steel beams in the comparison with the beams reinforced by FRP bars. However, specific reinforcement ratios A_f/A_s used to show the feasibility of the hybrid FRP-steel RC beams compared with the steel RC beams could not be proposed in this section due to the lack of analytical data. Thus, to obtain the deep understanding on the effect of reinforcement ratio A_f/A_s on the structural response and the ductility of concrete beams reinforced with FRP and steel tension bars, the parametric study for this ratio should be carried out.

In conclusion, the FE method is an effective tool to accurately predict various features, including the load-deflection relationship, stress evolution in FRP and steel reinforcement, failure mode, strain distribution and crack propagation of concrete beams reinforced with both steel and FRP tension reinforcements. In addition, the stiffness of the concrete beams reinforced with FRP-steel bars is well assessed through the FE simulation. Moreover, the ductility evaluation of the hybrid FRP-steel RC beams by means of absorption energy is also feasible through the FE simulation.

4. Parametric study on member ductility by finite element (FE) analysis

The reliability of FE simulations for the hybrid FRP-steel RC beams has been confirmed in Chapter 3. Therefore, the extensive FE model specimens with various parameters have been prepared making beam specimen B4 the reference specimen. The objective of this chapter is to extend and enhance the discussion on how to improve the member ductility by providing optimum parameters.

4.1 Design of parametric investigation

The investigated parameters are the reinforcement ratios together with the concrete compressive strength and the FRP types, and the arrangement of the tension reinforcement. To consider the effect of the reinforcement arrangement, the FE models B4_Diff. level with the FRP bars in the outer layer of two layers of tension reinforcement are created to compare with the original B4_Same level (FRP bars in one layer of reinforcement) evaluated in Chapter 3. For the FE models of the beam B4 with different levels, the vertical spacing from the center of FRP bars to the center of the steel bars is changed with the values of 10, 20 and 30 mm. To consider the safety requirement, the four beams with the different gaps (a = 0, 10, 20, 30 mm) between FRP and steel bars are designed with the same flexural strength of 140 kN, as shown in **Table 4** and **Fig. 12(a)**. On the other hand, the designed beams for the parametric study on the influences of the reinforcement ratios together with the concrete compressive strength and the FRP types are described in **Table 4** and **Fig. 12(b)**. The load-carrying capacities by bending theory of the beams in

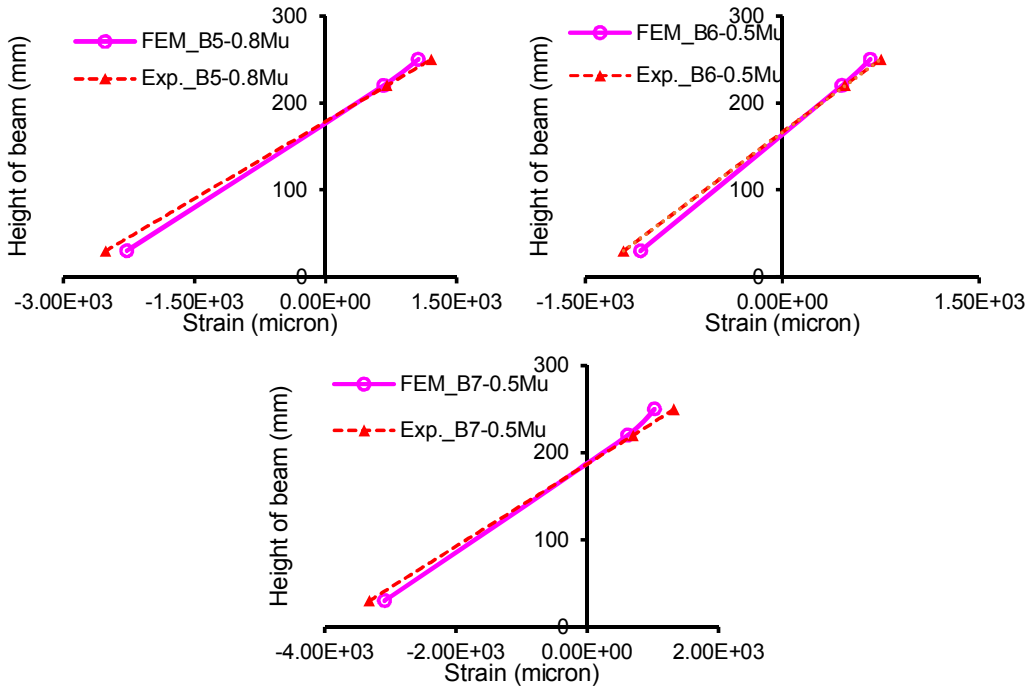

Fig. 11 Comparison between tested and simulated results in strain distribution.

Table 4 Details of the parametric study on reinforcement ratios, concrete compressive strength and types of FRP, and simulated absorption energy and yielding load.

Group	Beam ID	A_s (mm^2)	A_f (mm^2)	$\rho_r = A_f/A_s$	E_f (MPa)	f_f (MPa)	f_c' (MPa)	Absorption energy (kNmm)	Yielding load (kN)
Group 1	B4_G1_R1	157.08	452.39	2.880	41000	755	33.1	2586.0	57
	B4_G1_R2	200.96	396.91	1.975	41000	755	33.1	2602.0	63
	B4_Diff. level_a = 10 mm	200.96	427.65	2.128	41000	755	33.1	3279.4	66
	B4_Diff. level_a = 20 mm	200.96	461.81	2.298	41000	755	33.1	3469.4	65
	B4_Diff. level_a = 30 mm	200.96	490.87	2.443	41000	755	33.1	3627.6	68
	B4_G1_R3	254.46	314.16	1.235	41000	755	33.1	2569.5	73
	B4_G1_R4	307.88	307.88	1.000	41000	755	33.1	2807.2	83
	B4_G1_R5	396.91	254.46	0.641	41000	755	33.1	2870.3	101
	B4_G1_R6	508.94	200.96	0.395	41000	755	33.1	2899.9	109
	B4_G1_R7_Steel	628.32	-	-	-	-	33.1	3515.5	136
	B4_G1_R8	200.96	1587.64	7.900	10250	755	33.1	2949.3	63
Group 2	B4_G2_R1	157.08	452.39	2.880	41000	755	44.5	1987.8	60
	B4_G2_R2	200.96	396.91	1.975	41000	755	44.5	2389.0	66
	B4_G2_R3	254.46	314.16	1.235	41000	755	44.5	2851.7	73
	B4_G2_R4	307.88	307.88	1.000	41000	755	44.5	2961.0	82
	B4_G2_R5	396.91	254.46	0.641	41000	755	44.5	3280.7	102
	B4_G2_R6	508.94	200.96	0.395	41000	755	44.5	3015.2	121
	B4_G2_R7_Steel	763.41	-	-	-	-	44.5	3590.1	149
Group 3	B4_G3_R1	157.08	452.39	2.880	41000	755	60.0	4588.4	58
	B4_G3_R2	200.96	396.91	1.975	41000	755	60.0	5173.2	65
	B4_G3_R3	254.46	314.16	1.235	41000	755	60.0	5546.2	76
	B4_G3_R4	307.88	307.88	1.000	41000	755	60.0	5966.9	86
	B4_G3_R5	396.91	254.46	0.641	41000	755	60.0	6780.6	101
	B4_G3_R6	508.94	200.96	0.395	41000	755	60.0	7529.1	125
	B4_G3_R7_Steel	804.25	-	-	-	-	60.0	7645.4	179
Group 4	B4_G4_R1	157.08	452.39	2.880	124000	1700	33.1	775.0	94
	B4_G4_R2	200.96	396.91	1.975	124000	1700	33.1	865.6	96
	B4_G4_R3	254.46	314.16	1.235	124000	1700	33.1	951.1	96
	B4_G4_R4	307.88	307.88	1.000	124000	1700	33.1	915.6	111
	B4_G4_R5	396.91	254.46	0.641	124000	1700	33.1	1282.6	120
	B4_G4_R6	508.94	200.96	0.395	124000	1700	33.1	1369.4	138
	B4_G4_R7_Steel	942.48	-	-	-	-	33.1	1646.7	160
	B4_G4_R8	200.96	150.80	0.750	124000	1700	33.1	1657.5	64
Group 5	B4_G5_R1	157.08	452.39	2.880	50100	1366	33.1	1313.9	60
	B4_G5_R2	200.96	396.91	1.975	50100	1366	33.1	1354.2	65
	B4_G5_R3	254.46	314.16	1.235	50100	1366	33.1	1294.9	76
	B4_G5_R4	307.88	307.88	1.000	50100	1366	33.1	1252.4	86
	B4_G5_R5	396.91	254.46	0.641	50100	1366	33.1	1497.9	104
	B4_G5_R6	508.94	200.96	0.395	50100	1366	33.1	1511.0	120
	B4_G5_R7_Steel	763.41	-	-	-	-	33.1	1728.9	145
	B4_G5_R8	200.96	339.29	1.688	50100	1366	33.1	2214.0	63

each group are similar, and the values of 140 kN, 160 kN, 190 kN, 150 kN, and 145 kN are computed for the flexural capacities of the beam specimens in the groups 1, 2, 3, 4, and 5, respectively. Furthermore, to investigate the effect of FRP types on the flexural performance of hybrid FRP-steel beams, the three beam specimens B4_G1_R8 (proposed FRP), B4_G4_R8 (CFRP) and B4_G5_R8 (AFRP) are designed for group 1, group 4 and group 5 with the same flexural strength as the beam B4_G1_R2 (GFRP) in group 1. Groups 1-3 are designed to investigate the effects of the hybrid reinforcement ratio for three cases of the concrete compressive strength. Groups 1, 4, 5 are employed to investigate the effects of the hybrid reinforcement ratio for three types of FRP reinforcement. In addition, the failure mode of all beams in **Table 4** is the concrete crushing in which the compressive strain exceeds 0.003, after steel yields.

4.2 Effect of reinforcement ratios among concrete compressive strength and FRP types

In **Figs. 13(a)**, **(b)**, **(c)** and **14(a)**, **(b)**, there is a clear correlation between the load-deflection performance

and the reinforcement ratio. In general, it is obvious from the aforementioned figures and **Table 4** that the mechanical performances of the ductility, absorption energy and initial stiffness of the reference steel RC beams are better than those of the hybrid FRP-steel RC beams. In the hybrid FRP-steel beams, FRP tension reinforcement is employed to take up the flexural strength while the steel reinforcement is mainly responsible for improving the ductility requirement. As displayed in **Table 4** and drawn in **Fig. 17**, the values of absorption energy of the simulated beams generally increase as the hybrid reinforcement ratios ($\rho_r = A_f/A_s$) decrease and the concrete beams reinforced with single steel tension bars provide the highest absorption energy values in each group. However, in several cases, the absorption energy values of the beams with a high hybrid reinforcement ratio are greater than those of the specimens with a low hybrid reinforcement ratio, implying that the fracture energy was affected by not only the hybrid reinforcement ratio but also the mechanical properties of the concrete and FRP bars. By observing the values of energy in each beam group in **Table 4**, the minimum absorption energy of the hybrid FRP-steel RC beams in each group is found in the beam with the hybrid reinforcement ratio of 2.880, which is approximately 47-76% of absorption energy of the corresponding reference beam. From **Table 4**, the conditions of the energy of the hybrid FRP-steel beams achieve the 80% of the absorption energy of the steel RC beams with the same flexural strength as follows. In the case of the beams reinforced by FRP and steel tension bars with concrete compressive strength of 33.1 MPa, the hybrid reinforcement ratios (A_f/A_s) are respectively no greater than 0.641, 0.395 and 0.641 for GFRP, CFRP and AFRP types. Due to the very high elastic modulus of CFRP, the displacement and the ultimate load of the beams with CFRP and steel bars are respectively lower and greater than those with GFRP/AFRP (low elastic modulus) and steel bars. Additionally, the steel reinforcement plays an important role in the ductility displacement of the hybrid FRP-steel RC beams. Therefore, to obtain the good ductility that is defined by absorption energy, the reinforcement ratio of CFRP to steel contents in the hybrid CFRP-steel RC beams is lower than the reinforcement ratio of the beams with GFRP/AFRP and steel tension bars. In the case of
beams reinforced with GFRP and steel tension bars, the hybrid reinforcement ratios (A_f/A_s) that are no greater

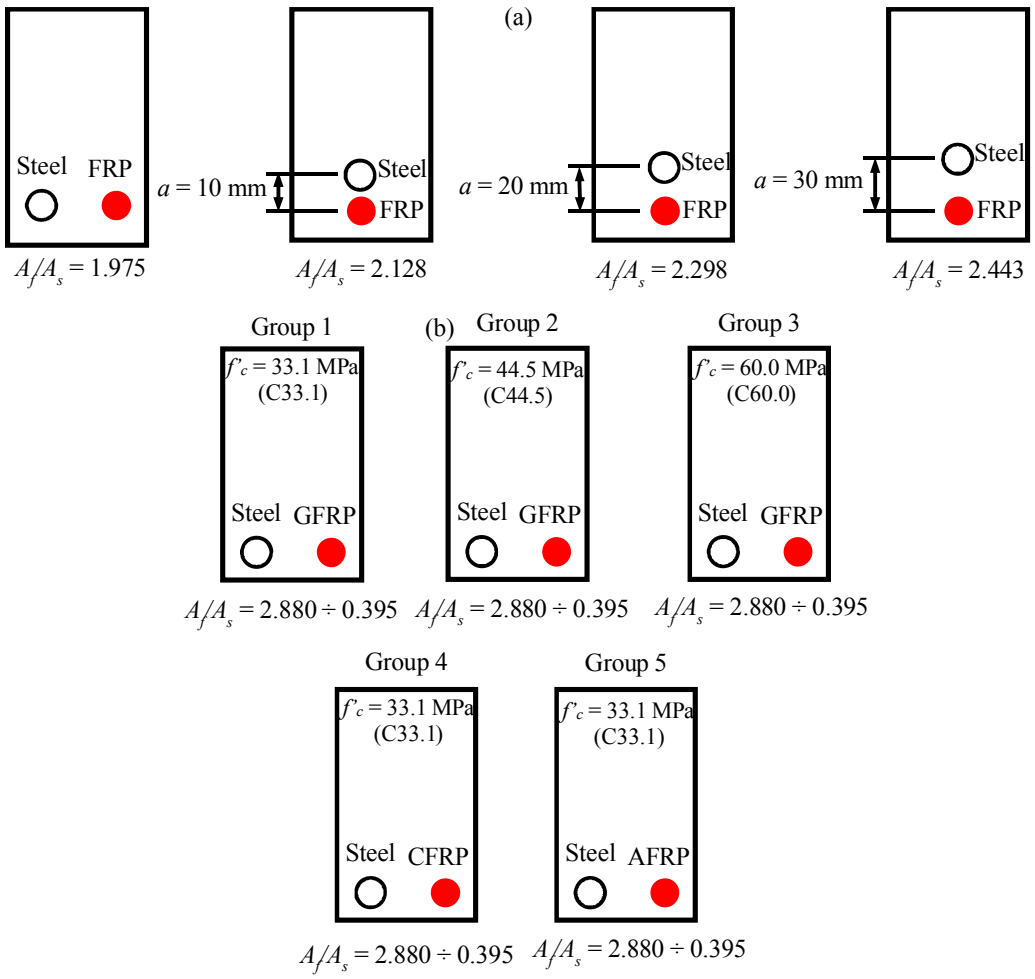

Fig. 12 (a) Reinforcement arrangement cases, and (b) cases of reinforcement ratios among concrete compressive strength and FRP types (each group has a steel RC beam with the same flexural capacity design).

than 0.641, 1.000 and 0.641 for the corresponding concrete strength of 33.1 MPa, 44.5 MPa and 60.0 MPa should be provided to achieve 80% of the absorption energy of the
corresponding steel RC beams. Under the contribution of concrete, as observed from **Figs. 13(a)**, **(b)**, **(c)** and **Table 4**, with the higher concrete compressive strength, the yielding load and the deformation are greater. Together with the increase in concrete strength, the use of a low hybrid reinforcement ratio makes the yielding load of the beams achieve high level. Therefore, the absorption energy
of the beams with high concrete strength and low hybrid reinforcement ratio is high, and the ductility of those beams is improved. The findings described above indicate that together with reinforcement ratio (A_f/A_s), the concrete strength and the FRP types affect the ductility of beams with hybrid use of steel and FRP reinforcement. However, the lower hybrid reinforcement ratios A_f/A_s result in the higher initial rigidity, which is clearly shown in **Figs. 13 -14** and is rather explicit in the cases using the GFRP and AFRP bars for the partial tension reinforcement. Due to the very high elastic modulus of carbon fiber-reinforced polymer (CFRP) bars, the initial stiffness of the hybrid CFRP-steel RC beams is clearly indistinct by reducing the reinforcement ratio A_f/A_s.

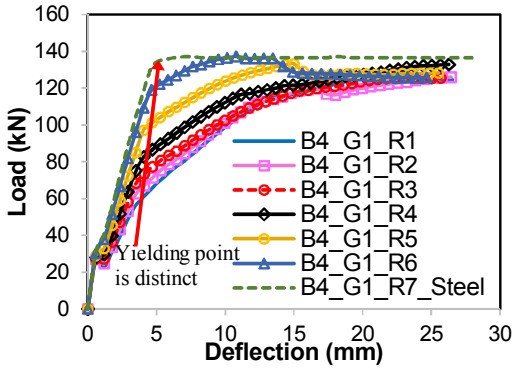

(a) Effect of hybrid reinforcement ratio (with concrete strength of 33.1 MPa)

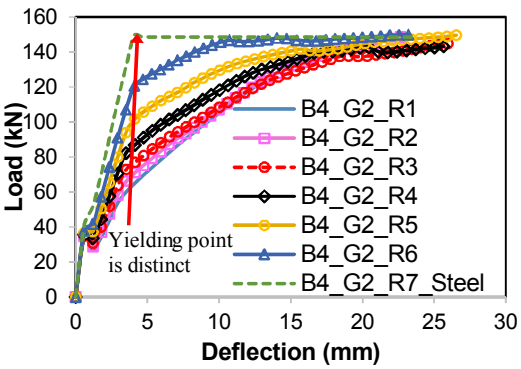

(b) Effect of hybrid reinforcement ratio (with concrete strength of 44.5 MPa)

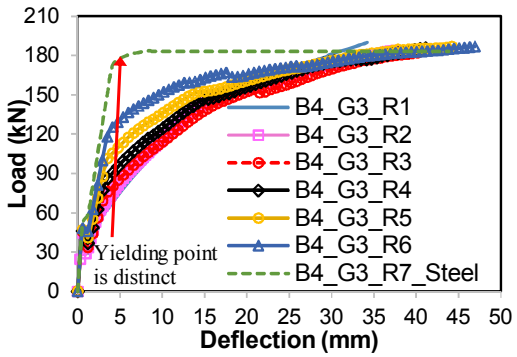

(c) Effect of hybrid reinforcement ratio (with concrete strength of 60.0 MPa)

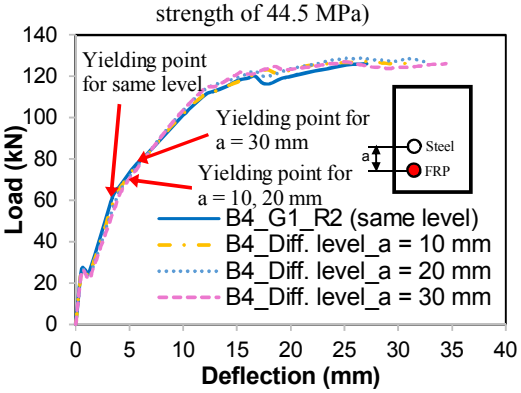

(d) Effect of reinforcement positions

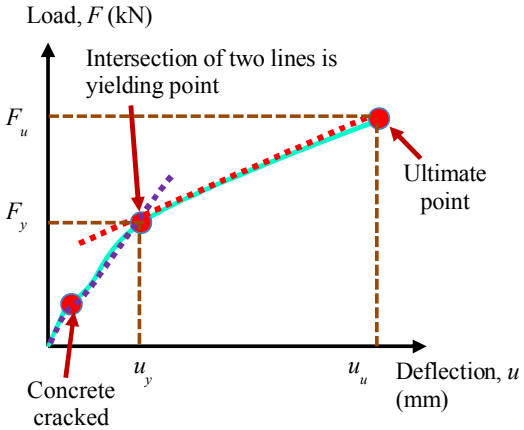

(e) Method to define the yielding point of a hybrid FRP-steel RC beam

Fig. 13 Effect of hybrid reinforcement ratio with different concrete compressive strengths and effect of reinforcement arrangement.

Table 5 Effects of reinforcement arrangement and types of FRP reinforcement.

Parameter	Specimen	A_s (mm^2)	A_f (mm^2)	$\rho_r = A_f/A_s$	Designed ultimate load (kN)	FEM ultimate load (kN)	Difference in load (%)
FRP types	B4_G1_R2 (GFRP)	200.96	396.91	1.975	140	127	NA
	B4_G4_R8 (CFRP)	200.96	150.80	0.750	140	131	3.14
	B4_G5_R8 (AFRP)	200.96	339.29	1.688	140	126	0.79
	B4_G1_R8 (FRP proposed)	200.96	1587.64	7.900	140	127	0.00
Reinforcement arrangement	B4_G1_R2 (same level)	200.96	396.91	1.975	140	127	NA
	B4_Diff. level_a = 10 mm	200.96	427.65	2.128	140	127	0.00
	B4_Diff. level_a = 20 mm	200.96	461.81	2.298	140	126	0.79
	B4_Diff. level_a = 30 mm	200.96	490.87	2.443	140	126	0.79

Table 5 (continued)

Parameter	Specimen	Ultimate deflection (mm)	Difference in deflection (%)	Yielding load (kN)	Absorption energy (kNmm)
FRP types	B4_G1_R2 (GFRP)	27.05	NA	63	2602.0
	B4_G4_R8 (CFRP)	17.90	33.83	64	1657.5
	B4_G5_R8 (AFRP)	23.00	14.97	63	2214.0
	B4_G1_R8 (FRP proposed)	27.84	2.92	63	2949.3
Reinforcement arrangement	B4_G1_R2 (same level)	27.05	NA	63	2602.0
	B4_Diff. level_a = 10 mm	31.59	16.78	66	3279.4
	B4_Diff. level_a = 20 mm	32.90	21.63	65	3469.4
	B4_Diff. level_a = 30 mm	34.40	27.17	68	3627.6

Generally, with a higher ratio of A_f/A_s, the load-carrying capacity of the hybrid FRP-steel RC beams can be enhanced as well as the FRP reinforcement tending to suffer higher tensile forces after the steel yielded. From **Figs. 13(a) - (c)** and **Figs. 14(a) - (b)**, the yielding point, which is defined in **Fig. 13(e)** and revealed in **Tables 4** and **5**, of the simulated beams is distinctly defined by decreasing the hybrid reinforcement ratio A_f/A_s; therefore, the yielding load is relatively smaller than the ultimate load of the beams with the low ratio of FRP to steel tension bars, increasing the ductility of those specimens.

4.3 Effect of reinforcement arrangement

The behavior of the four concrete beams reinforced with the different positions of FRP and steel bars is determined in **Fig. 13(d)**. Clearly, the responses in terms of the service conditions, before 60% of the ultimate load, of the four specimens B4_G1_R2 (same level) and B4_Diff. level are clearly similar. However, the slope of load-deflection curves of those beams is changed at the high load level. Specifically, the initial rigidity of specimen B4_G1_R2 (same level) is slightly higher than that of specimens B4_Diff. level_a = 10, 20, and 30 mm. Furthermore, **Table 5** shows that the load-carrying capacity of beams reinforced by the different levels of tension bars is almost the same as that of the concrete member with the same level of GFRP and steel reinforcement. In the FE simulation, however, the maximum deflection of the hybrid beams with the two layers of bars is increased by 16.78%, 21.63%, and 27.17% with the increase in the gap between the steel and FRP reinforcement in comparison with the reference specimen, B4_G1_R2 (same level). Under the condition of the same flexural strength and the same failure mode of concrete crushing after steel yields, the beams reinforced with larger gap between FRP and steel bars result in the greater effective depth to FRP reinforcement. Hence, the tensile force of the FRP bars is small for the specimens with larger FRP to steel reinforcement distances, and the maximum deflection of those specimens is therefore increased. Since the ultimate deflection increases as the gap between the FRP and steel bars increases, the absorption energy of the hybrid FRP-steel beams with larger gap of FRP to steel bars is enhanced, as shown in the last column of **Table 5**. Therefore, **Fig. 13(d)** indicates that the larger gap between the steel and FRP reinforcement shows an improvement in ductility for the hybrid beams rather than the smaller spacing between steel and FRP bars. Moreover, the hybrid beams with greater spacing of FRP to steel bars reveal that the yielding load of steel reinforcement, which is indicated in **Fig. 13(d)** and **Table 5**, was relatively small compared to the ultimate load, increasing the ductility of those beams that were also improved in the comparison with the beams reinforced by the smaller gap between FRP and steel bars. From the aforementioned discussions, comparing the hybrid beams with the same level of FRP and steel reinforcement, the strength, rigidity and ductility of the hybrid FRP-steel RC beams can be compensated by providing more FRP and placing the steel and FRP bars at the different levels in the tension zone with the large distance between FRP and steel reinforcement. Moreover, the corrosion of steel reinforcement is mitigated by arranging the different level of reinforcement in which FRP bars are placed in the outer layer and steel bars are laid in the inner layer.

4.4 Effect of FRP types

For the effects of the FRP type on the load-deflection

response, ultimately applied load and midspan deflection results of the simulated hybrid beams are shown in **Fig. 14(c)** and **Table 5**. The hybrid reinforcement ratios (A_f/A_s) of the investigated specimens B4_G1_R2 (group 1), B4_G1_R8 (group 1), B4_G4_R8 (group 4) and B4_G5_R8 (group 5) of **Table 4** are 1.975, 7.990, 0.750 and 1.688, respectively. Moreover, those analyzed specimens contained the same steel reinforcement amount, A_s = 200.96 mm^2. The FRP-steel RC beam B4_G1_R8 employs FRP bars whose rupture strain is four times that of the GFRP and whose elastic modulus is one-fourth that of the GFRP. Clearly, the initial response of the three specimens reinforced with the GFRP, CFRP and AFRP bars is relatively similar. However, the slope of load-deflection curves of those beams is changed after the cracking of the concrete. Specifically, the stiffness of the specimen reinforced by CFRP-steel bars is greater than the stiffness of the beams reinforced with AFRP/GFRP and steel rods, due to the higher elastic modulus of CFRP bars. In **Fig. 14(c)**, as expected, the B4_G4_R8 (CFRP) and B4_G5_R8 (AFRP) models achieve the similar load-carrying capacities to the control beam B4_G1_R2 (GFRP) with values obtained in range from 126 kN to 131 kN of failure load. However, the maximum deflections of the hybrid CFRP-steel and AFRP-steel RC beams are dropped by 33.83% and 14.97% in the comparison with the beam reinforced by GFRP-steel bars. Under the same flexural strength and the same failure mode of concrete crushing of the investigated specimens, the aforementioned finding may be mainly due to the lower elastic modulus of GFRP, which results in a greater deformation, compared to those of AFRP and CFRP. By using the same ductility definition as the case of the effect of reinforcement arrangement, a lack of ductility is easily recognized in the concrete beams reinforced with CFRP and steel tension bars since the energy absorption of those beams is lower than the energy absorption of the concrete beams with hybrid use of AFRP/GFRP and steel reinforcement (see the last column of **Table 5** for the values of energy absorption). Additionally, the high elastic modulus and the low fracturing strain of CFRP rods make the hybrid CFRP-steel RC members stiff and brittle; therefore, the beams reach the peak load at a low displacement, then fail immediately by concrete crushing. The contribution of the elastic moduli of CFRP bars is significant in the load-carrying capacity and rigidity of the hybrid beams. However, this effect causes a negative influence on the ductility consideration of the hybrid members. With the highest value of the absorption energy, the concrete beams reinforced by GFRP and steel bars improve the ductility since the lower elastic modulus and the higher fracturing strain of GFRP bars allow the contribution of steel reinforcement on the ductility of the hybrid GFRP-steel beam to be heavily utilized. By comparison to the steel RC beams with the same flexural capacity, the

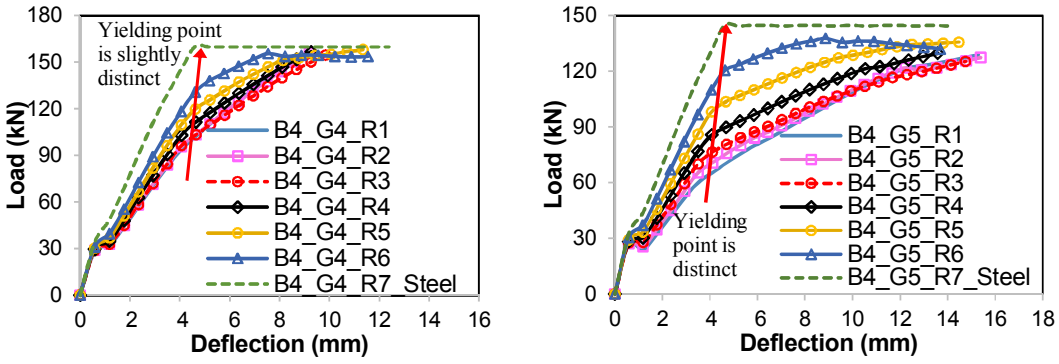

(a) CFRP (b) AFRP

(c) A comparison of effect of FRP types, E_f (GFRP) = 41 GPa, E_f (proposed FRP) = 10.25 GPa, E_f (CFRP) = 124 GPa and E_f (AFRP) = 50.1 Gpa

Fig. 14 Effect of reinforcement ratio together with FRP types.

Table 6 Absorption energy, ductility factor and ductility index of the experimental results.

Authors	Beam ID	Absorption energy (kNmm)	Ductility factor, u_u/u_y	Ductility index $(\Delta u/u_u)/(\Delta F/F_u)$
Aiello and Ombres (2002)	A1	3516.0	6.92	1.56
	A2	3401.4	6.08	1.70
	A3	9576.8	4.08	2.29
Qu *et al.* (2009)	B1	1816.9	3.08	8.76
	B2	2520.9	-	-
	B3	2669.4	4.78	2.15
	B4	2330.8	8.42	1.73
	B5	2864.8	5.87	2.98
	B6	2512.3	4.82	2.80
	B7	1892.4	11.00	1.65
	B8	1777.8	1.61	0.53
Lau and Pam (2010)	G0.6-T1.0-A90	13920.6	4.19	1.89
	G1.0-T0.7-A90	19025.4	3.86	1.90
	G0.3-MD1.0-A90	6506.0	7.28	1.99

concrete beam reinforced by GFRP and steel bars can achieve 74% of the absorption energy of the steel RC beams. Furthermore, the absorption energy of the hybrid FRP-steel RC beam B4_G1_R8, in which the mechanical property of reinforced FRP bars is proposed above, can reach 83% of the absorption energy of the reference beam reinforced with single steel bars under the same flexural strength. Therefore, the property of the FRP bars employed in specimen B4_G1_R8 with 10.25 GPa of Young's modulus (one-fourth of the GFRP elastic modulus) and 7.36% of the rupturing strain (four times the GFRP fracturing strain) can be a better option than GFRP for practical use.

In conclusion, the strength and stiffness of FRP bars can be compensated by providing more FRP reinforcement. However, the low fracturing strain, which is a weak point of carbon and aramid fibers, cannot be substituted by any. Thus, the beams reinforced with FRP, such as GFRP which has a low elastic moduli and high rupturing strain, and steel bars imply a better ductility than the beams with hybrid CFRP/AFRP and steel reinforcement. In addition, a Young's modulus of 10.25 GPa and a fracturing strain of 7.36% is proposed for the property of FRP tension reinforcement in the concrete beams with hybrid use of FRP and steel bars to achieve an absorption energy close to that of the reference steel RC beam under the same load carrying capacity.

4.5 Ductility-related indices

Aside from the ductility corresponding to the area under the load-displacement curves, as explained above, the current study uses the ductility factor defined by the ratio of ultimate displacement to yielding deflection. This work also proposes a ductility index to discuss the ductility measurements of the concrete beams with the combination of FRP and steel tension reinforcement.

Figure 10 indicates that the behavior of concrete beams reinforced by FRP-steel bars was divided into the three stages. To consider the ductility of the beams, stage 2 and stage 3 were carefully investigated. Based on the consideration of the post-yield stiffness of the beams, which was also adopted in the study of Arafa *et al.* (2015) to assess the ductility behavior of the RC members, this research introduces a simple ductility index to evaluate the ductility of hybrid FRP-steel RC beams. Since the post-yield stiffness of a hybrid FRP-steel RC beam is almost decided by FRP reinforcement; therefore, the magnitude of the post-yield rigidity to whole stiffness ratio $[(\Delta u/u_u)/(\Delta F/F_u)]$ is correlated with the ductility of this beam. The $\Delta u = u_u - u_y$ (mm), $\Delta F = F_u - F_y$ (kN), and F_u, F_y, u_u, u_y correspond to the applied loads and deflections at the ultimate and steel yielding. As a ductility definition, the ductility of a beam is enhanced when the ductility index computed by $(\Delta u/u_u)/(\Delta F/F_u)$ increases.

Table 6 shows the results of the ductility of the hybrid FRP-steel RC beams in the literature defined according to the methods of conventional steel RC beams (ductility factor, u_u/u_y) and the index proposed in the present study. As defined in each index meaning, **Table 6** shows that the absorption energy of the tested beams is enhanced when the ductility index increases. This trend is observed in the studies of Qu *et al.* (2009) and of Lau and Pam (2010). **Table 6** also implies that beam B8 is the most brittle because of the smallest values of ductility factor, u_u/u_y, absorption energy and ductility index $(\Delta u/u_u)/(\Delta F/F_u)$. Beam B8 therefore fails immediately after steel yielding. For the beams A1, A2, and A3, the ductility index provides the same ranking with the calculated absorption energy. Clearly, beam A3 has the largest values of the fracture energy and the ductility index, $(\Delta u/u_u)/(\Delta F/F_u)$; thus, the most ductile beam is A3. However, the ductility evaluation of the tested specimens by adopting the ductility index and absorption energy in this study are different from that using the ductility factor defined as the conventional steel RC beams. These above findings are in complete agreement with the results obtained by Pang *et al.* (2015).

Additionally, the description of mechanical performance of hybrid FRP-steel RC beams in comparison with steel RC beam is carried out by comparing the three indices: ductility factor, ductility index and absorption

energy. The simulated results of the parametric study with the beams designed in **Table 4** are employed. **Figures 15**, **16** and **17** show the relationships between ductility indices, FRP types and concrete compressive strength varying among hybrid reinforcement ratios of the analyzed beams. Moreover, the exponential function regression is applied to draw the trend lines of those relationships. From **Figs. 15** and **17**, under the same flexural capacity in each beam group, it is similar to the trend of absorption energy defined in the previous sections, in which the ductility index values decreased as the hybrid reinforcement ratios A_f/A_s increased. The ductility index of the steel RC beams is much higher than that of the hybrid FRP-steel members since the post-yield response of those reference specimens is nearly horizontal, implying that with the same load carrying capacity, a hybrid FRP-steel beam could be ductile if its post-yield stiffness is close to that of the corresponding steel RC beam. This finding can be obtained through the beams resulting in high yielding load and large ultimate displacement, in which the corresponding absorption energy of those specimens is high. In the contrast to the aforementioned observations, the ductility defined by the ductility factor of the hybrid FRP-

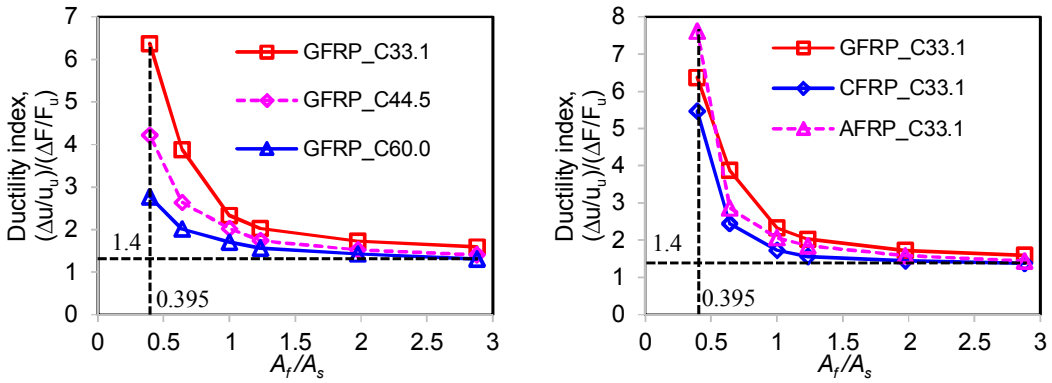

(a) Effect of concrete strength (b) Effect of FRP types

Fig. 15 Relationship of reinforcement ratio and ductility index in the beams of parametric study.

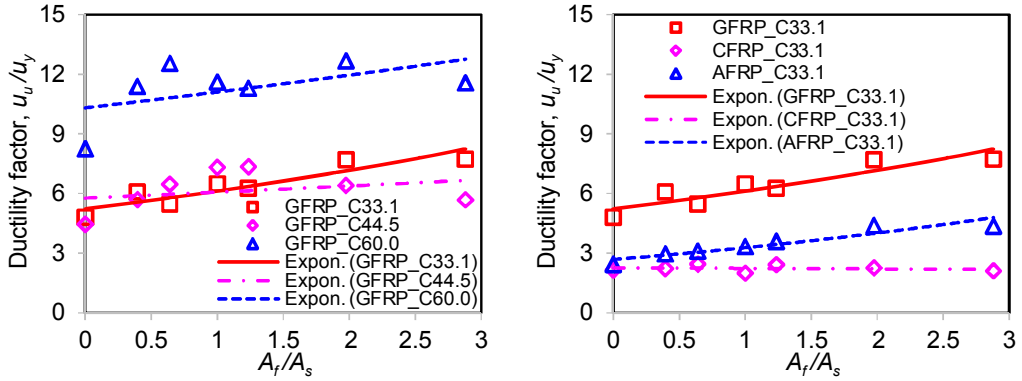

(a) Effect of concrete strength (b) Effect of FRP types

Fig. 16 Relationship of reinforcement ratio and ductility factor in the beams of parametric study.

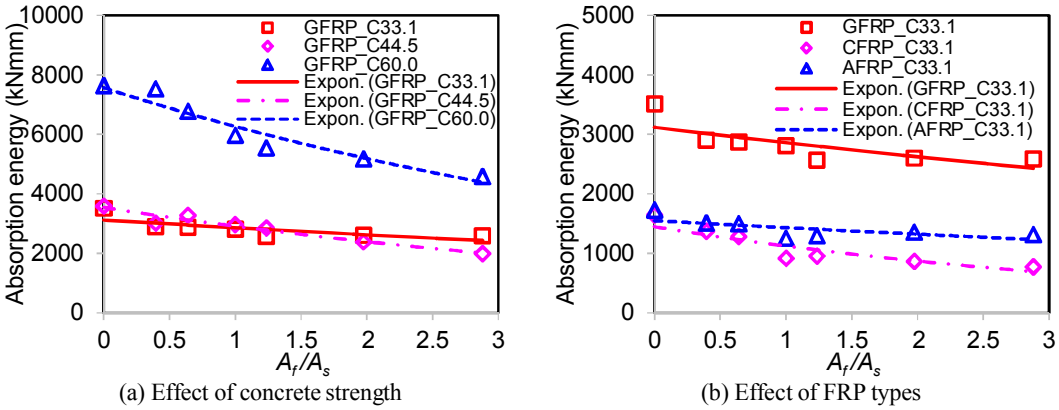

(a) Effect of concrete strength (b) Effect of FRP types

Fig. 17 Relationship of reinforcement ratio and absorption energy in the beams of parametric study.

steel RC beams is slightly enhanced as the hybrid reinforcement ratio increases. Moreover, by using the ductility factor and absorption energy, **Figs. 16(a)** and **17(a)** indicate that the ductility indices are reduced by decreasing the concrete compressive strength. This finding is completely opposite to the values defined by the ductility index (as seen in **Fig. 15(a)**). From **Figs. 15(b)**, **16(b)** and **17(b)**, the results computed by the three ductility indices of the GFRP-steel RC beam are generally greater than those of the AFRP-steel and CFRP-steel RC beams.

Based on the observations from **Figs. 15** and **17**, the practical feasibility of the hybrid FRP-steel RC beams through the requirement of the ductility index, which requires the 80% of the absorption energy of the steel reference beams, is expressed as follows. The hybrid FRP-steel RC beams with concrete compressive strength of 33.1 MPa should hold the ductility index $(\Delta u/u_u)/(\Delta F/F_u)$ to no less than 3.88, 5.47 and 2.87 for the GFRP, CFRP and AFRP types, respectively. To provide these ductility index values sufficiently, the hybrid reinforcement ratio A_f/A_s is required to be not larger than 0.641 for the beams with GFRP/AFRP-steel cases and that ratio is also recommended to be no greater than 0.395 for the specimens reinforced with CFRP-steel bars. In the case of the beams reinforced with GFRP and steel tension bars, the ductility indices $(\Delta u/u_u)/(\Delta F/F_u)$ that are no less than 3.88, 2.03 and 2.01 should be ensured for the corresponding concrete strengths of 33.1 MPa, 44.5 MPa and 60.0 MPa. To satisfy these ductility requirements, the hybrid reinforcement ratio A_f/A_s should be controlled to be no greater than 0.641 for concrete strength ranging from 33.1 to 60.0 MPa. On the other hand, the minimum ductility index of 1.40 corresponding to 47% of the steel RC beam absorption energy can be achieved for a concrete compressive strength ranging from 33.1 to 60.0 MPa, the FRP types with the elastic moduli from 41 to 124 GPa and the hybrid reinforcement ratio from 0.395 to 2.880.

5. Conclusions

This study gains insight into the mechanical performance and the ductility of concrete beams reinforced by FRP and steel tension bars. The reliability of the FE modeling is validated through comparing the simulated results to the experimental data for the beams tested in the previous studies. Additionally, an extensive parametric study is also carried out by means of the FE program to analyze the ductility of the hybrid FRP-steel RC beams by providing optimum experimental parameters. From the numerical investigation, the following conclusions can be drawn.

(1) Based on the FE simulation results of the available data, the FE models can predict the load-deflection relationships of the hybrid FRP-steel RC beams well with a maximum deviation less than 10% in the load-carrying capacity and the displacement. The stiffness of the beams simulated by the FE method is higher than those of the experimental results mainly due to the perfect bond assumption between the reinforcement and concrete. In addition, the FE tool also simulates the failure mode of concrete crushing after steel yielding of the hybrid FRP-steel RC beams well. On the other hand, the FE results indicate the difference on the role of FRP and steel reinforcement in a hybrid RC beam. In fact, the FRP bars are mainly responsible for the ultimate strength of the hybrid RC beam, while the ductility performance of that specimen is almost concentrated on the steel reinforcement. Therefore, the ductility defined by absorption energy of the FRP-steel RC beam could be enhanced if the hybrid reinforcement ratio A_f/A_s is small.

(2) From the parametric study, generally, the use of the high strength concrete and the low hybrid reinforcement ratio A_f/A_s offers the enhancement on the ductility defined by the absorption energy of the hybrid FRP-steel beams. In addition, the beams reinforced with the larger gap between FRP and steel bars in the tension zone provide a better ductility in the comparison with the hybrid beams with the smaller spacing between FRP and steel reinforcement. The ductility defined through the fracture energy of the hybrid FRP-steel RC beams is improved when the FRP bars with low elastic modulus and high rupturing strain (such as GFRP) are employed. Indeed, based on the simulated results, the FRP property with 10.25 GPa of Young's modulus (one-fourth that of GFRP) and 7.36% of rupturing strain (four times that of GFRP) can achieve over 80% of the absorption energy of the reference steel RC beams.

(3) A simple and reliable ductility index is proposed to evaluate the ductility of concrete beams reinforced with steel and FRP bars. This ductility index displays a similar observation of the absorption energy concept in the ductility performance. Similar to the results obtained from the absorption energy, the ductility index values decrease as the hybrid reinforcement ratios A_f/A_s increase. Under the same flexural capacity condition, the absorption energy of the hybrid FRP-steel RC beams can achieve 80% of that of the steel reference beams when the following requirements on the ductility index are sufficiently offered. For the hybrid beams with concrete strength of 33.1 MPa, the ductility index values are no less than 3.88, 5.47 and 2.87 for the GFRP, CFRP and AFRP types, and the corresponding hybrid reinforcement ratios are no greater than 0.641 (for the GFRP and AFRP cases) and 0.395 (for the CFRP case). In addition, the ductility indices $(\Delta u/u_u)/(\Delta F/F_u)$ that are no less than 3.88, 2.03 and 2.01 for the corresponding concrete strength of 33.1 MPa, 44.5 MPa and 60.0 MPa should be ensured for the concrete beams reinforced by GFRP and steel

bars, attained when the hybrid reinforcement ratio of FRP to steel bars is less than or equal to 0.641. On the other hand, the minimum ductility index of 1.40 of the beams analyzed in this work can be achieved by at least 47% of the absorption energy of the corresponding steel RC beams.

Acknowledgments

This study was financially supported by the ASEAN University Network/Southeast Asia Engineering Education Development Network-AUN/SEED-Net.

References

ACI 440.1R-06, (2006). "*Guide for the design and construction of structural concrete reinforced with FRP bars*." Detroit: American Concrete Institute, USA.

Aiello, M. A. and Ombres, L., (2002). "Structural performances of concrete beams with hybrid (Fiber-Reinforced Polymer-Steel) reinforcements." *Journal of Composites for Construction*, 6(2), 133-140.

ANSYS – Release Version 15.0, (2013). "*A finite element computer software and user manual for nonlinear structural analysis.*" Canonsburg, USA.

Arafa, M. A. I., Zhishen W., Mohamed F. M. F. and Doaa K., (2015). " Experimental study on cyclic response of concrete bridge columns reinforced by steel and basalt FRP reinforcements." *Journal of Composites for Construction*, 20(3), 1-19.

Bencardino, F., Condello, A. and Ombres L., (2016). "Numerical and analytical modeling of concrete beams with steel, FRP and hybrid FRP-steel reinforcements." *Composite Structures*, 140, 53-65.

Bischoff, P. H., (2007). "Deflection calculation of FRP reinforced concrete beams based on modifications to the existing Branson equation." *Journal of Composites for Construction*, 11(1), 4-14.

Branson, D. E. (1977), *Deformation of Concrete Structures*, McGraw-Hill, New York, USA.

Faza, S. S. and GangaRao, H. V. S., (1993). "Theoretical and experimental correlation of behaviour of concrete beams reinforced with fiber plastic rebars", *Fiber Reinforced Plastic Reinforcement for Concrete Structures*, SP-138, American Concrete Institute, Detroit, 599-614.

Ge, W., Zhang, J., Cao, D. and Tu, Y., (2015). "Flexural behaviors of hybrid concrete beams reinforced with BFRP bars and steel bars." *Construction and Building Materials*, 87, 28-37.

Godat, A., Labossière, P., Neale, K. W. and Chaallal, O., (2012). "Behavior of RC members strengthened in shear with EB FRP: Assessment of models and FE simulation approaches." *Computures & Structures*, 92-93, 269-282.

Hawileh, R. A., (2015). "Finite element modeling of reinforced concrete beams with a hybrid combination of steel and aramid reinforcement." *Materials & Design*, 65, 831-839.

Hognestad, E., Hanson, N. W. and McHenry D., (1955), "Concrete stress distribution in ultimate strength design." *ACI Journal Proceedings*, 52(12), 455-479.

Kara, I. F., Ashour, A. F. and Köroğlu, M. A., (2015). "Flexural behavior of hybrid FRP/steel reinforced concrete beams." *Composite Structures*, 129, 111-121.

Kara, I. F., (2016). "Flexural performance of FRP-reinforced concrete encased steel composite beams." *Structural Engineering and Mechanics,* 59(4), 775-793.

Lau, D. and Pam, H. J., (2010). "Experimental study of hybrid FRP reinforced concrete beams." *Engineering Structures*, 32(12), 3857-3865.

Linh, V. H. B., Boonchai, S. and Ueda, T., (2017). "Mechanical performances of concrete beams with hybrid usage of steel and FRP tension reinforcement." *Computers and Concrete*, 20(4), 391-407.

Oller, E., Marí, A., Bairán, J. A. and Cladera, A., (2015). "Shear design of reinforced concrete beams with FRP longitudinal and transverse reinforcement." *Composites Part B: Engineering*, 74, 104-122.

Pang, L., Qu, P., Zhu, P. and Xu, J., (2015). "Design propositions for hybrid FRP-steel reinforced concrete beams." *Journal of Composites for Construction*, 20(4), 1-9.

Qin, R., Zhou, A. and Lau, D., (2017). "Effect of reinforcement ratio on the flexural performance of hybrid FRP reinforced concrete beams." *Composites Part B: Engineering*, 108, 200-209.

Qu, W., Zhang, X. and Huang, H., (2009). "Flexural behavior of concrete beams reinforced with hybrid (GFRP and steel) bars." *Journal of Composites for Construction*, 13(5), 350-359.

Tan, K. H., (1997). "Behavior of hybrid FRP-steel reinforced concrete beams." In: *Proceeding 3rd International Symposium on Non-Metallic (FRP) Reinforcement for Concrete Structures (FRPRCS-3)*, Japan Concrete Institute, Tokyo, 487-494.

Yoo, D. Y. and Banthia, N., (2015). "Numerical simulation on structural behavior of UHPFRC beams with steel and GFRP bars." *Computers and Concrete*, 16(5), 759-774.

Yoo, D. Y., Banthia, N. and Yoon, Y. S., (2016). "Flexural behavior of ultra-high-performance fiber-reinforced concrete beams reinforced with GFRP and steel rebars." *Engineering Structures*, 111, 246-262.

Zhang, D., Ueda, T. and Furuuchi, H., (2012). "A design proposal for concrete cover separation in beams strengthened by various externally bonded tension reinforcements." *Journal of Advanced Concrete Technology*, 10, 285-300.

Zhang, D., Wang, Q. and Dong, J., (2016). "Simulation study on CFRP strengthened reinforced concrete beam under four-point bending." *Computers and Concrete*, 17(3), 407-421.